XXI IMEKO World Congress "Measurement in Research and Industry"
August 30 - September 4, 2015, Prague, Czech Republic

Ultrathin transparent photodetector for use in Standing-Wave Interferometer.

Ingo Ortlepp[1], Hans-Joachim Büchner[1], Tzvetan Ivanov[2], Manuel Hofer[2], Jens-Peter Zöllner[2], Ivo Rangelow[2], Eberhard Manske[1]

[1] Institute of Process Measurement and Sensor Technology, Technische Universität Ilmenau, D-98693 Ilmenau, Germany, info.pms@tu-ilmenau.de
[2] Group: Microelectronic and Nanoelectronic Systems, Technische Universität Ilmenau, D-98693 Ilmenau, Germany, jens-peter.zoellner@tu-ilmenau.de

Abstract - A novel photodiode for application in a standing-wave interferometer was developed. The operation principle is based on the optical standing wave whose stationary intensity profile can be detected by a photosensor which - for this purpose - has to be transparent and thinner than the optical wavelength. The working principle and basic design requirements of the developed sensor are described, and the results of measurements inside and outside the standing wave are discussed.

Keywords: standing wave, interferometer, photosensor, photodiode, transparent

1. INTRODUCTION

In the field of length measurement with high accuracy and high resolution, interferometric measurement principles are of great importance. Interferometers are used in high-precision machines such as coordinate measuring machines, wafer steppers and for calibration [1, 2, 3]. However, due to the complex setup of most conventional interferometers consisting of numerous optical parts they require single-part production and elaborate adjustment which makes them comparatively expensive. Because of the limited potential for miniaturisation of the optical components the crosswise setup of the popular Michelson-Interferometer leads to a certain minimum overall size.

Sensors for Standing-Wave Interferometry enable a completely new concept for interferometers. As standing-wave interferometer heads only consist of a mirror, two photosensors and a collimator, they allow easy alignment, small design and inexpensive mass production.

1.1. The Standing-Wave Interferometer

The existence of standing waves is well described in literature [4, 5] and was first investigated by Wiener [6].

When an optical wave is reflected by a plane mirror, the reflected beam undergoes a phase shift of π and then interferes with the incident beam in opposite direction. The field intensities E_{in} and E_{re} of both beams superpose, resulting in the standing-wave field intensity E_{sw}:

$$E_{\mathrm{sw}} = E_{\mathrm{in}} + E_{\mathrm{re}}. \tag{1}$$

The intensity I_{sw} of the standing wave can be derived as follows:

$$I_{\mathrm{sw}} = 2I_0 \left(1 - \cos\left(\frac{4\pi}{\lambda} z\right)\right) \tag{2}$$

with the intensity of the incident beam I_0, wavelength λ and direction of propagation z. It can be seen from (2) that I_{sw} varies from 0 (destructive interference) to $4I_0$ (constructive interference). As a result of the phase shift, the field intensity on the reflective surface is zero at any time, causing the profile of intensity to be phase-coupled to the mirror.

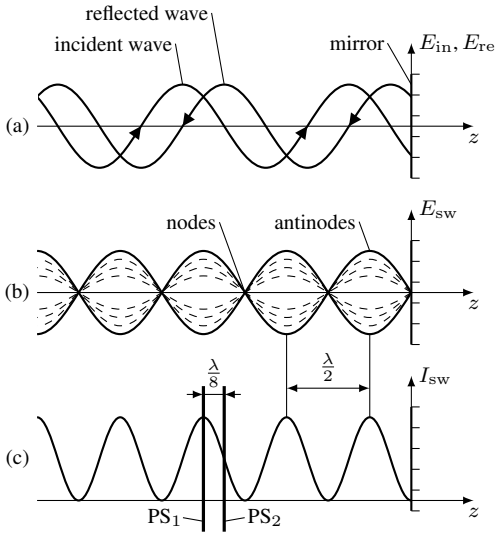

Fig. 1. (a) Field intensities E_{in}, E_{re} of incident and reflected wave. (b) Phase shift of π of the reflected wave causes node in E_{sw} of resulting standing wave to be coupled to the mirror. (c) Intensity of standing wave, minimums corresponding to nodes, maximums to antinodes of E_{sw}. Periodicity of intensity is $\lambda/2$. I_{sw} can be sampled by two photosensors PS$_1$ and PS$_2$.

The intensity profile can be detected by a photosensor, which – for this purpose – has to be transparent and thinner than the optical wavelength [7, 8]. When the mirror and the sensor are moved relative to each other along the optical axis, the intensity profile pervading the sensor will shift, resulting in a pulsating photosignal s. To recognise the moving direction, a second photosensor with a distance of $(2k-1)\frac{\lambda}{8}$, $(k \in \mathbb{Z})$ with respect to the first one has to be placed in the optical path, so quadratursignals can be obtained (Fig. 1c).

The interferometers utilising the described principles and sensors can be considerably miniaturised. Due to the simple linear structure and the small number of necessary parts the minimum overall size is only slightly larger than the laser beam diameter (see Fig. 2).

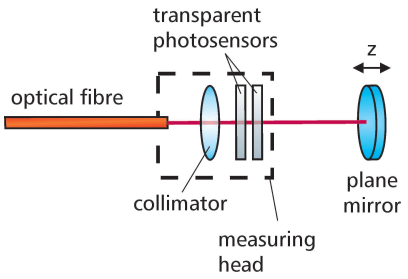

Fig. 2. Structure of a standing-wave interferometer. The complexity is considerably reduced compared with an industrial Michelson interferometer.

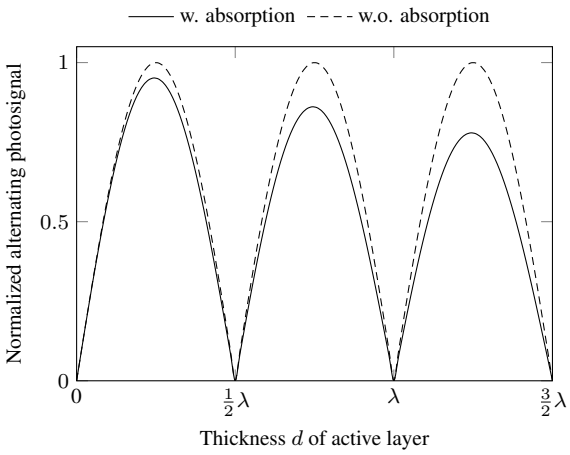

Fig. 3. Alternating component of photosignal as function of the thickness of active layer. The height of the maxima is decreasing at thicknesses $d > \frac{\lambda}{2}$ due to absorption and the resulting increase of the direct component s_-.

1.2. Sensor properties

As the photosensor affects the standing wave itself, there are some requirements for a beneficial detection of the intensity profile.

First, the photosensor has to be sufficiently transparent. With decreasing transparency the photosignal s would otherwise experience a growing offset s_- while the desired alternating component $s_\sim$ diminishes. As the real photosensor is not perfectly transparent, there will always be a direct component in the photosignal s:

$$s = s_\sim + s_- \tag{3}$$

Second, the thickness d of the active, photosignal-generating layer has to fulfil certain requirements as d directly influences the photosignal. The following issue should be taken into account: The whole active layer volume is pervaded by the standing wave, so the sensor integrates the intensity profile within its boundaries. Considering the shape of I_{sw} (2), there are two extremal thicknesses. The first one is $d = 0$, for which the sensor signal would vanish completely. The second extremum is a thickness of $k\frac{\lambda}{2}$ which means the sensor integrates over one or more entire intensity periods. This will lead to a sensor signal consisting of the direct component s_- only, while $s_\sim = 0$. In both cases the generated photosignal is not applicable for determining the movement of the mirror or the sensor, so a thickness aside the discussed extrema should be applied. As there will be a race condition between thickness of the active layer, sensor transparency and the amplitude of the generated photosignal, this issue is subject to optimisation. Fig. 3 shows the normalised alternating component of the photosignal as a function of the active layer thickness d. When absorption is taken into account, the optimal thickness is $d = \frac{\lambda}{4}$.

Third, also the antireflection coating of the transparent sensor has to be considered. For adequate operation, the sensor must be adjusted perpendicular to the optical axis and, therefore, parallel to the mirror. This builds up an optical cavity (Fabry-Pérot setup) between the sensor surface and the mirror. As this cavity is placed within the optical path, it will affect the primary standing wave due to undesired multiple beam interferences. These interferences will degenerate the otherwise sinusoidal sensor signal, resulting a poor signal contrast (small $s_\sim$) and harmonics. To prevent this influence, the reflections must be sufficiently suppressed by an antireflection coating of the sensor.

1.3. State-of-the-Art

The first application of standing waves by Wiener [6] was a static one. The aim was to prove the existence of standing waves and the phase jump on reflective surfaces with the help of photoplates. An approach to use the optical standing wave for interferometric length measurements is described by Büchner in [9]. In this patent, the fundamental design of a standing-wave interferometer, consisting of a laser source, a mirror and two consecutively arranged, 90° phase-shifted sensors for bidirectional counting is presented. In [10, 11], Sasaki et al. propose a transparent photosensor based on a silicon on quartz substrate. In this sensor, two photodiodes are arranged side by side. The phase shift for bidirectional counting is accomplished by locally etching the quartz substrate, thus modifying the optical path length for one photodiode by $\frac{\pi}{2}$. Bunte et al. [12, 13] and Mandryka et al. [14, 15] introduce an interferometer based on a standing-wave sensor which is manufactured by silicon deposition on a glass substrate, thus forming two vertically stacked n-i-p photodiodes. The sensor is built up by the successive deposition of the appropriate layers (transparent conductive oxide and n-, i-, p-amorphous silicon) for the two photodiodes. A phase shift of $\frac{\pi}{2}$ and an inherent antireflection coating are achieved by an adequate selection of the individual layer thicknesses. An application of standing-wave sensors in a Fourier spectrometer is described by Knipp et al. [16], [17]. The sensor used is a

photoconductor fabricated by the deposition of amorphous silicon on a quartz wafer. Lazar et al. [18, 19] propose a photoresistive sensor consisting of a fused silica substrate with an active polycrystalline silicon layer and a set of antireflection coatings. They demonstrate a combined intra-cavity displacement measurement and simultaneous laser wavelength stabilisation onto this cavity.

2. WORKING PRINCIPLE

The transparent photosensor is carried out as ultrathin lateral p-i-n photodiode with a striped doping pattern (Fig. 4 and Fig. 5). The active area has the size of the laser beam ($l \approx 1\,\mathrm{mm}$) and an overall thickness of app. $600\,\mathrm{nm}$, including passive silicon oxide layers. The optimal thickness of the active layer is $d = \frac{\lambda}{4}$ (cf. Fig. 3). For silicon with $n = 3.8$ and $\lambda_0 = 633\,\mathrm{nm}$ this leads to

$$d = \frac{\lambda_0}{4n} = 42\,\mathrm{nm}. \tag{4}$$

The width w of the doped stripes affects the attainable photosensitivity (generated photocurrent per intensity). For the described sensor, w is subject to an optimisation between the path length for the charge carriers and the resulting capacity of the striped pattern. A width of $w = 10\,\mu\mathrm{m}$ turned out to be the optimum for the given technological parameters. The main reason for choosing a comb-shaped pattern is the resulting junction capacity. This capacity is far smaller for the chosen pattern than for a vertically stacked p-i-n layer diode as described in [20], so better dynamic properties can be expected.

The sensor is operated as regular photodiode in photoconductive mode, so when the sensor is illuminated, charge carriers are generated in the i-zone and transported to the p- and n-zones, resulting in a photocurrent i proportional to the irradiation intensity. As described above, the intensity of the standing wave varies along the optical axis, thus the relative axial movement between the mirror and the sensor generates a pulsating photocurrent consisting of an alternating component $i_\sim$ and a direct component i_-:

$$i = i_\sim + i_- \tag{5}$$

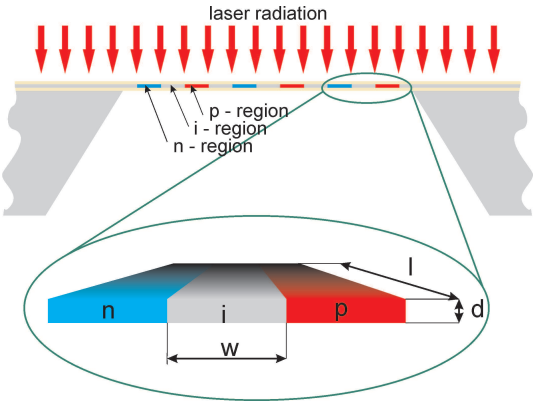

Fig. 4. Cross-section of photosensor. The active layer is carried out as ultra-thin silicon membrane ($d \approx 40\,\mathrm{nm}$), made by back-etching of an SOI wafer. The striped doping pattern forms a p-i-n photodiode for sensing I_{sw}.

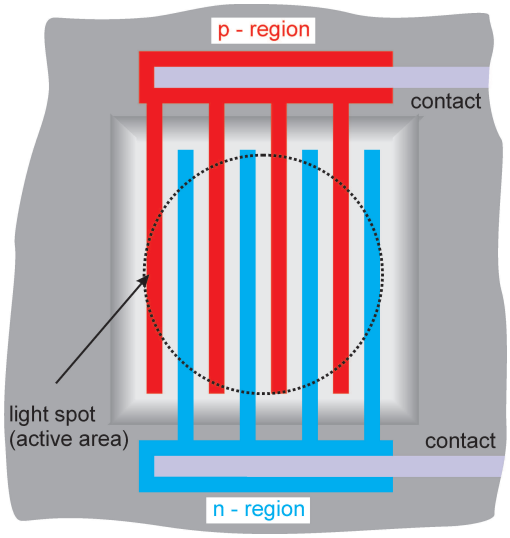

Fig. 5. Top view of photosensor. The transparent active area is app. $1\,\mathrm{mm} \times 1\,\mathrm{mm}$ and contains comb-shaped p- and n-doped areas to reduce the necessary diffusion length of the charge carriers generated in the i-zone (white). The p- and n-regions aside the active area are contacted by Al-stripes leading to bond-pads.

3. FABRICATION

3.1. Processing

For the manufacturing of the transparent photosensors monocrystalline silicon is used. It has an adequate absorption rate in the relevant spectral range and a low volume recombination rate due to the perfect lattice structure. Furthermore, the electrical properties of the respective regions can be adjusted according to the specific task by doping procedures without drastically changing the refractive index. A Passivation of the boundary surfaces can easily be achieved by an oxidation of the base material. The silicon planar technology allows the processing of local, well-defined surface areas and, thus, the realisation of a lateral photodiode structure. Doping procedures such as diffusion or ion implantation are perfectly suitable for manufacturing the described design. SOI-wafers with a silicon layer thickness of $100\,\mathrm{nm}$–$200\,\mathrm{nm}$ are used for manufacturing the sensors. After an oxidation (scattering oxide) of appr. $100\,\mathrm{nm}$, the n^+-regions for the ion implantation are defined by photolithography, and the implantation is carried out with phosphor as dopant. Afterwards, the photoresist is removed and the p^+-regions are processed in the same way, using boron as dopant. After the removal of the scattering oxide , a new isolation layer is applied. The conducting paths are defined in a further photolithography step. An aluminium film is deposited and, afterwards, structured by a lift-off or etching process. To

reduce undesired reflections from the sensor surface, an antireflection coating is applied to the top side of the wafer. After that, a glass plate is bonded in place for the mechanical stabilisation of the ultrathin transparent membrane formed in the next step. To achieve the necessary sensor transparency, the silicon substrate on the bottom side is locally thinned in the region of the sensor element by inductively coupled plasma reactive ion etching (ICP-RIE). Finally, a second antireflection coating is applied to the bottom side of the sensor. Fig. 6 shows a finished sensor.

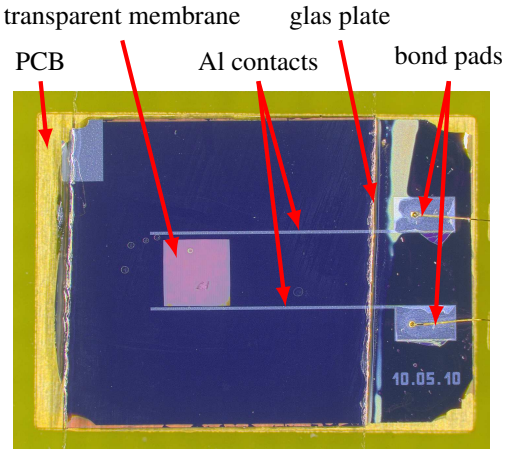

Fig. 6. Photo of finished sensor with glass plate stabilising the ultrathin membrane. The sensor is glued to a PCB for easier handling and connecting.

3.2. Flatness of membrane

A challenging characteristic of the sensor is the ultrathin photoactive membrane. For the best compromise between overall signal strength, signal contrast and optical transparency the thickness has to be $d = \frac{\lambda}{4}$, which is appr. $40\,\mathrm{nm}$ for the conditions mentioned above.

In addition to that, the membrane has to be absolutely flat. As the generated photocurrent is an integration over the entire volume of the active layer, with increasing deformation, the generated photocurrent i has its sources at several phase angles of I_{sw} resulting in a decreasing pulsating component $i_{\sim}$. Depending on the actual shape, at a planarity error of $e_{\mathrm{p}} \approx \frac{\lambda}{2}$ the alternating sensor signal $i_{\sim}$ would vanish, because the standing-wave intensity is integrated over an entire period, resulting in a signal only consisting of i_{-}.

For an acceptable signal contrast and low offset, the maximum permissible planarity error is $e_{\mathrm{p}} \leq \frac{\lambda}{4}$. To accomplish this value, the membrane has to be bonded onto a glass substrate before the final etching process. For the adhesive there are several requirements arising from the application. These are transparency, temperature stability for the subsequent processing steps, refractive index similar to glass, low viscosity and chemical stability.

3.3. Antireflection-coating

To prevent multiple-beam interferences between sensor and mirror, the reflectance of the sensor has to be sufficiently low. The preferred approach was to design the layer thicknesses of the sensor in a way that the reflectance is acceptably low without additional coatings ('inherent' AR). However, due to technological and physical restrictions (section 1) as well as the commercial availability of wafers, the thicknesses of the sensor layers could not be selected arbitraryly. For this reason inherent AR was impeded for the given basic conditions, thus making additional coatings necessary.

These coatings are carried out as thin films, deposited by physical vapour deposition (PVD) on both sides of the sensor membrane. Thereby, the theoretical reflectance could be reduced from $R = 49.8\,\%$ for the uncoated sensor with best possible inherent AR to $R = 0.06\,\%$ for the AR-coated sensor with matched basic layers.

4. EXPERIMENTAL RESULTS

4.1. Diode characteristic

Primarily the diode behaviour of the sensors produced has been investigated. This has been done done after each process step once the wafer is p- and n- doped as well as the bond pads are connected. Degrading electric properties indicate undesired process results, thus allowing better control over the production process. The sensors produced show a good diode behaviour with reverse current of appr. $1\,\mathrm{nA}$.

4.2. Photo-sensitivity and linearity

For a reasonable detection of the standing wave intensity and possible subsequent interpolation of the electrical signal, the photosensors need both adequate photosensitivity and linearity. The photosensitivity p is the ratio of generated photocurrent i and incident optical power P_{opt}:

$$p = \frac{i}{P_{\mathrm{opt}}} \tag{6}$$

For an ideal photodiode p is constant for all incident P_{opt}. For real photodiodes there are deviations from that ideal relation due to several effects. These deviations are reflected in the sensor linearity. Photosensitivity and linearity are determined in a combined measurement. For this purpose a modulated diode laser source is used to illuminate the sensor. A ramp-shaped modulation signal is applied to the laser focused on the sample under test. To eliminate side effects caused by non-linearities of the laser source, the emitted optical power is split and monitored by a reference receiver (laser power meter). The sensor is actuated in short-circuit operation, and the signal is amplified using a commercial transimpedance amplifier.

The measured photosensitivities range from $0.71\,\mu\mathrm{A\,mW^{-1}}$ to $2.1\,\mu\mathrm{A\,mW^{-1}}$. For an application in a standing-wave interferometer with a He-Ne-laser (appr. $1\,\mathrm{mW}$) the achieved photosensitivity yields a feasible signal strength. The measured linearity error is shown in Fig. 7.

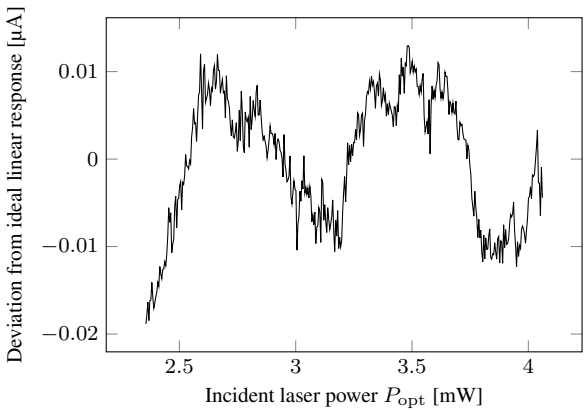

Fig. 7. Linearity error of the sensor, measured by modulating the diode laser.

4.3. Frequency response

The intended utilisation of the sensors in an interferometric setup entails also dynamic demands. When applying a relative movement between the mirror and the sensor, the intensity profile pervading the sensor will shift. The sensor response to the pulsating variation of intensity has to be fast enough in order to eliminate fringe counting errors in the subsequent evaluation electronics. Generally, a maximum measuring speed of $v_{\mathrm{meas}} = 1\,\mathrm{m\,s^{-1}}$ can be considered sufficient for most applications, resulting in a necessary cut-off frequency f_{c} of

$$f_{\mathrm{c}} = \frac{2 v_{\mathrm{meas}} n_{\mathrm{air}}}{\lambda_0} = 3\,\mathrm{MHz} \tag{7}$$

for a laser wavelength of $\lambda_0 = 633\,\mathrm{nm}$ and the refrative index of air $n_{\mathrm{air}} = 1$.

The cut-off frequency measurements are not performed in a standing-wave setup due to the arduous realisation of high mirror velocities. Instead, a modulated laser diode was used and the emitted beam was monitored with a commercial high-speed photodiode as reference receiver. The developed sensors show cut-off frequencies up to 70 MHz, corresponding to a possible measuring velocity $v_{\mathrm{meas}} > 20\,\mathrm{m\,s^{-1}}$.

4.4. Experiment in the standing wave

For the experimental work on the optical standing wave a setup as shown in Fig. 8 and Fig. 9 was used. There, a fibre-coupled stabilised He-Ne-Laser is adjusted perpendicular to a mirror. Exact alignment is indicated by the destabilisation of the laser due to back reflections into the optical fibre. In order to prevent those destabilising back reflections during subsequent measurements, a Faraday isolator is inserted in the optical path. To apply relative movement between the standing-wave photodetector and the mirror, a piezo actuator is attached to the roller guide carrying the mirror and modulated with a sinusoidal signal. The modulation voltage is chosen so that the mechanical amplitude is in the size of several λ. Afterwards, the standing-wave sensor is mounted in place and adjusted for maximum signal amplitude.

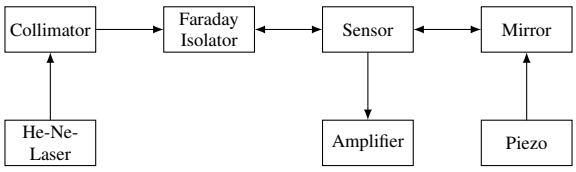

Fig. 8. Experimental setup for application of the sensor in the standing wave. The laser source is a stabilized, fibre-coupled He-Ne-Laser. A piezo actuator is used to apply movement to the mirror, thus the standing wave is shifted through the sensor, inducing a pulsating photocurrent.

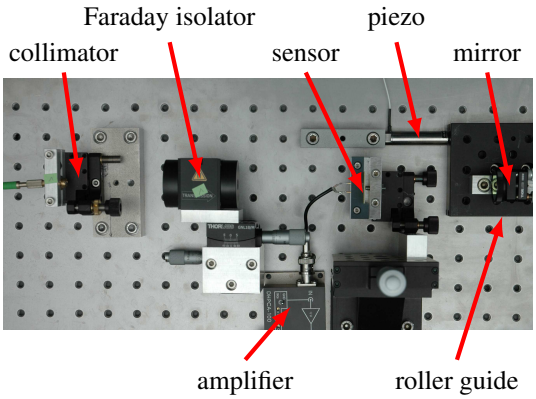

Fig. 9. Standing-wave setup.

The attained signal of the described setup is shown in Fig. 10. It can be seen that the generated photocurrent consists of two components i_{-} (1.1 µA) and $i_{\sim}$ (1.6 µA) as described in section 2. The displayed discontinuities in the sinusoidal signal result from the mechanical direction reversal of the piezo actuator which causes a phase reversal in the observed photosignal.

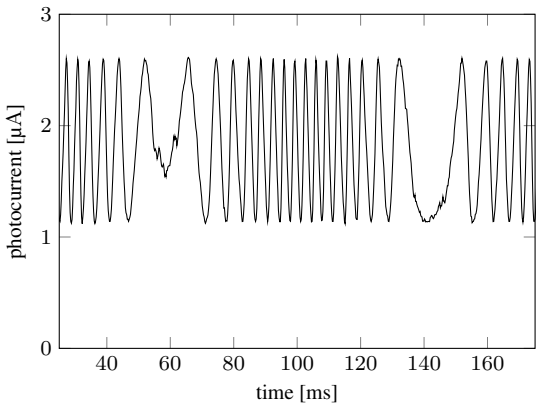

Fig. 10. Photo current of sensor operated in the optical standing wave.

For interpolation purposes the generated sensor signal has to be an ideal sine, otherwise the necessary phase measurement for subdividing the period of I_{sw} will experience a phase error. To determine the quality of the sensor signal, a FFT of an interval between two discontinuities (see Fig. 10) was calculated. The resulting spectrum shows a narrow peak at 450 Hz. A small

harmonic at 900 Hz is observable, which indicates multi beam interferences in between the sensor layers or the sensor and the mirror due to undesired reflections.

5. CONCLUSIONS and OUTLOOK

A novel sensor for application in an optical standing-wave interferometer has been developed and investigated. The sensor consists of an ultrathin photoactive layer, implemented as p-i-n photodiode, which detects the standing wave intensity profile. The comb-shaped doping design results in a small junction capacity of the photodiode, leading to cut-off frequencies up to 70 MHz. To achieve a sufficient flatness of the ultrathin membrane, it is bonded to a glass plate before thinning. Furthermore, additional antireflection coatings are applied to the sensor to prevent undesired multiple beam reflections between sensor and mirror, which would otherwise degenerate the primary standing wave. Finally, the linearity of the sensor signal and the signal in a standing-wave interferometer setup are investigated.

For continuing development of the sensor, investigations on improving the membrane flatness are currently carried out. These involve different membrane designs as well as adhesives preferably with a very low viscosity to reduce stress on the membrane during the bonding process. A flatter membrane will result in a lower signal offset and a larger alternating signal component.

The final step will be the integration of a second sensor in the standing-wave setup. An appropriately adjusted distance of the two sensors will result in phase shifted photosignals, allowing bidirectional counting.

ACKNOWLEDGEMENTS

The project was funded by the German Federal Ministry of Education and Research under contract 03V0235.

REFERENCES

[1] H. A. M. Spaan, R. L. Donker and I. Widdershoven, "Isara 400: development of an ultra-precision CMM for 3D measurement of large parts", *Proceedings of the ASPE spring topical conference*, 2009.

[2] G. Jäger, E. Manske, T. Hausotte and H. J. Büchner, "Nanomessmaschine zur abbefehlerfreien Koordinatenmessung (Nano Measuring Machine for Zero Abbe Offset Coordinate-measuring)", *Tm Technisches Messen Plattform für Methoden, Systeme und Anwendungen der Messtechnik*, 67.7-8/2000, 319, 2000.

[3] C. R. Steinmetz, "Sub-micron position measurement and control on precision machine tools with laser interferometry", *Precision Eng.* 12 12–24, 1990.

[4] E. Hecht, *Optik*, 5. Ed., Oldenbourg Wissenschaftsverlag GmbH, 2009.

[5] H. Haferkorn, *Optik*, 4. Ed., Wiley-VCH, 2003.

[6] O. Wiener, "Stehende Lichtwellen und die Schwingungsrichtung polarisirten Lichtes", *Ann. Phys.*, 276: 203–243, 1890.

[7] H. Stiebig et al., "Standing wave detection by thin transparent n–i–p diodes of amorphous silicon", *Thin solid films*, 427(1), 152-156, 2003.

[8] H. J. Büchner, H. Stiebig, V. Mandryka, E. Bunte and G. Jäger, "An optical standing-wave interferometer for displacement measurements", *Measurement science and technology*, 14(3), 311, 2003.

[9] H. Büchner, "Stehende-Wellen-Interferometer zur Messung von optischen Gangunterschieden.", *Deutsches Patent* DE 3300369, 1983.

[10] M. Sasaki, X. Mi, and K. Hane, "Standing wave detection and interferometer application using a photodiode thinner than optical wavelength." *Applied Physics Letters*, 75.14, 2008-2010, 1999.

[11] Y. Li, X. Mi, M. Sasaki and K. Hane, "Precision optical displacement sensor based on ultra-thin film photodiode type optical interferometers.", *Measurement Science and Technology*, 14(4), 479, 2003.

[12] E. Bunte, V. Mandryka, K. Jun, H. Büchner, G. Jäger and H Stiebig, "Thin transparent pin-photodiodes for length measurements", *Sensors and Actuators A: Physical*, 113.3, 334-337, 2004.

[13] E. Bunte, K. Jun, and H. Stiebig, "Micro interferometer based on amorphous silicon nanosensor.", *Journal of Optoelectronics and Advanced Materials*, 7.4, 1899-1907, 2005.

[14] V. Mandryka, H. Büchner and G. Jäger, "Design aspects in the development of a standing wave interferometer.", *Proc. SPIE* 5457, Optical Metrology in Production Engineering, 175, 2004.

[15] H. Büchner, E. Bunte, V. Mandryka, H. Stiebig and G. Jäger, "Standing-wave interferometer based on partially transparent photodiodes", *Proc. SPIE* 5144, Optical Measurement Systems for Industrial Inspection III, 218, 2003.

[16] H. Kung, S. Bhalotra, J. Mansell, and D. Miller, "Compact transform spectrometer based on sampling a standing wave." *Red*, 100.150, 200, 2000.

[17] D. Knipp, et al., "Silicon-based micro-Fourier spectrometer.", *Electron Devices, IEEE Transactions on*, 52.3, 419-426, 2005.

[18] M. HOLÁ et al., "Nanopositioning with detection of a standing wave.", *NANOCON 2013. International Conference /5.*, 2013.

[19] J. Lazar et al. "Interferometry with Stabilization of Atmospheric Wavelength.", *X IMEKO TC14 Symposium on Laser Metrology for Precision Measurement and Inspection in Industry*, Braunschweig, Germany, Sept. 2011.

[20] K. H. Jun, E. Bunte and H. Stiebig, "Optimization of phase-sensitive transparent detector for length measurements", *Electron Devices, IEEE Transactions on*, 52(7), 1656-1661, 2005.

[21] E. Manske et al., "New applications of the nanopositioning and nanomeasuring machine by using advanced tactile and non-tactile probes", *Measurement Science and Technology*, 18(2), 520, 2007.